Computers and Chemical Engineering 133 (2020) 106633

Contents lists available at ScienceDirect

Computers and Chemical Engineering

journal homepage: www.elsevier.com/locate/compchemeng

Adaptive flux variability analysis of HEK cell cultures

Thomas Abbate[a], Laurent Dewasme[a], Alain Vande Wouwer[a,*], Philippe Bogaerts[b]

[a] Automatic Control Laboratory, University of Mons, 31 Boulevard Dolez, Mons 7000, Belgium
[b] Université libre de Bruxelles, Brussels School of Engineering, 3BIO-BioControl, Av. F.D. Roosevelt 50 C.P. 165/61, Brussels 1050, Belgium

ARTICLE INFO

Article history:
Received 15 August 2019
Revised 2 November 2019
Accepted 3 November 2019
Available online 9 November 2019

Keywords:
Metabolix flux analysis
Metabolic network
Mathematical modelling
HEK cells
Biotechnology

ABSTRACT

Measured external fluxes impose constraints to under-determined metabolic networks that narrow the internal flux intervals obtained using Flux Variability Analysis. Nevertheless, these constraints often lead to systems that do not admit a feasible solution. Measurement noise and data smoothing are among the sources of uncertainties that can cause system infeasibility. These constraints are classically released using interval representation of fluxes. This study investigates the use of Adaptive Flux Variability Analysis (AFVA), which allows determining a minimal coefficient of variation of the external fluxes along the time course of the experiment. Especially, AFVA is applied to a medium-size metabolic network and a rich dataset relative to HEK-293 cells cultured in batch, encompassing all 20 amino acids and less commonly measured metabolites, such as urea and pyruvate. AFVA appears as an effective tool for metabolic flux analysis. The impact of data-smoothing and the information provided by the cell growth are thoroughly analyzed.

1. Introduction

Several industrial processes make use of cell cultures technologies in order to manufacture various products of interest such as monoclonal antibodies, viral vectors, proteins, etc. To improve the understanding of cell metabolism and henceforth the efficiency of such processes, different cell lines have been extensively studied over the last decades (Heath and Kiss, 2007; Ravi et al., 2015). In this context, the parallel development of '-omics' technologies and computational tools has allowed reconstructing cellular metabolic networks and quantitatively characterizing the activity of well-known intracellular pathways (Duarte et al., 2007; Thiele and Palsson, 2010; Petiot et al., 2015; Kanehisa et al., 2016).

These computational tools can be classified into three categories (Trinh et al., 2009): metabolic flux analysis (MFA), flux balance analysis (FBA) and metabolic pathway analysis (MPA). MFA is applied when the considered networks become (over)determined with the addition of extracellular metabolite measurements. In some cases, this allows the computation of a unique solution (Stephanopoulos et al., 1998; Provost and Bastin, 2004). Nevertheless, the complexity of the metabolic networks often leads to under-determined systems and thus to an infinity of admissible solutions, even with the addition of an extensive number of measurements. FBA tackles this issue through the optimization of an objective function, such as the maximization of the growth rate (Kauffman et al., 2003; Price et al., 2004), which leads in some case studies to the selection of a unique solution among the solution space. In many other cases however, the system remains underdetermined with an infinity of flux distributions leading to the same minimum of the objective function. Instead of selecting one possible set of internal fluxes among the infinity of admissible solutions, MPA defines the intervals in which the intracellular fluxes are constrained. MPA includes elementary flux mode analysis (EFM) and extreme pathway analysis (EPA) that both define all existing pathways (succession of reactions) linking cell substrates and products, as well as the quantitative intervals in which internal fluxes are constrained. EPA differs from EFM in that it imposes that all extreme pathways are systematically independent (Trinh et al., 2009; Klamt and Stelling, 2003; Papin et al., 2004)). Extreme pathways therefore represent a subset of elementary modes.

In addition to traditional MPA methods, extreme admissible values of individual internal fluxes can be determined through computation of flux variability analysis (FVA) which consists in solving a simple linear programming problem (Leighty and Antoniewicz, 2011; Llaneras et al., 2012; Vercammen et al., 2014). While the usual analysis provides an insight into the cell activity under specific growth conditions, in the course of the exponential phase or the stationary phase for example, several studies provide a dynamic overview over the whole experiment using FBA

* Corresponding author.
E-mail addresses: thomas.abbate@umona.ac.be (T. Abbate), laurent.dewasme@umons.ac.be (L. Dewasme), alain.vandewouwer@umons.ac.be (A. Vande Wouwer), philippe.bogaerts@ulb.ac.be (P. Bogaerts).

https://doi.org/10.1016/j.compchemeng.2019.106633
0098-1354/

(Mahadevan et al., 2002), MPA (Fernandes et al., 2016; Zamorano et al., 2013) or FVA (Richelle et al., 2016; Bogaerts et al., 2017).

Even though FVA does not provide the whole set of potentially used internal pathway combinations as in MPA, this tool has the advantage of easily coping with measurement noise and data processing uncertainties (spline smoothing, differentiation, etc., potentially leading to the impossibility to satisfy the constraints imposed by both the network and the inferred extracellular fluxes), by considering flux intervals instead of unequivocally determined extracellular fluxes (Mahadevan and Schilling, 2003; Llaneras and Picó, 2007; Richelle et al., 2016). In the classical approach, however, the relative width of the intervals is constant over time and for all extracellular fluxes, regardless of the quality of the measured signals. This may lead to large admissible internal flux intervals. This issue is addressed in Abbate et al. (2019) where the authors develop a method called adaptive flux variability analysis (AFVA) which identifies, at each analysis time instant and possibly for each individual extracellular component, the minimum interval representation of fluxes that results in an admissible set of solutions. The user is therefore able to obtain a quantitative indicator of the impact of the measurement noise and indirect data processing, such as data smoothing, on the solution.

As the preliminary study (Abbate et al., 2019) is restricted to a small network presented in Bastin (2016), one of the objectives of the present work is to investigate the potential of AFVA with a larger network and extensive measurement datasets of HEK-293 cell cultures in batch mode. This cell line is widely used for the production of different viral vectors in the pharmaceutical industry and several metabolic network studies are available in the literature (Henry et al., 2005; Martinez et al., 2010; Henry et al., 2011; Quek et al., 2014; Karengera et al., 2017; Petiot et al., 2015). The present study considers a medium-size metabolic network with 82 reactions and 51 internal metabolites, including reversible reactions, and is based on a rich dataset encompassing all 20 amino acids and less commonly measured metabolites, such as urea and pyruvate.

Since AFVA has been developed to cope with uncertainties, a second objective of this work is to assess the impact of data smoothing on the analysis results.

A third objective is to investigate on how to account for the biomass growth rate estimation through viable cell concentration measurements, which often represents a very stringent (and therefore difficult to satisfy) constraint alongside the other inferred extracellular fluxes. This latter issue is usually tackled by considering intervals on the admissible growth rate. The present study proposes to use AFVA while imposing the biomass production rate as an external signal and to investigate how the biomass concentration can be reconstructed by integrating the resulting corrected biomass production rate.

The paper is organized as follows. The theory underlying FVA and AFVA is first introduced in Section 2. Next, the considered metabolic network and the experimental data used in this work are described in Sections 2.5 and 3. The several results are discussed in Section 4: a comparison between classical FVA and AFVA is achieved in Section 4.1, the impact of data-smoothing is assessed in Section 4.2 and results obtained when fixing the biomass flux are shown in Section 4.3. Conclusions are presented in Section 5.

2. Main concepts of flux variability analysis

In metabolic network analysis, the considered biological system usually consists in an entire cell or a cell compartment to which the principle of mass conservation of internal metabolites is applied. Within the system, metabolites transform into other metabolic intermediates through enzyme-catalysed reactions considered as internal reactions, or are transported inside and outside the system through exchange reactions (Trinh et al., 2009). The general equation of the internal metabolite dynamics can therefore be expressed as:

$$\frac{d\underline{C}}{dt} = N\underline{\nu} - \mu\underline{C} \tag{1}$$

where $\underline{C} \in \Re^m$ is the metabolite concentration vector expressed in (mmol/cell), $\underline{\nu} \in \Re^n$ is the vector of network fluxes, $N \in \Re^{(m \times n)}$ is the stoichiometric matrix where element $N_{i,j}$ is the stoichiometry coefficient relative to metabolite i taking part in reaction j, $\mu\underline{C}$ is the expression of the dilution that occurs due to cell growth and $\mu \in \Re$ is the specific growth rate.

This equation is then simplified using the assumption of slow/fast dynamics. On the one hand, the dilution term can be neglected in comparison with the internal and exchange reaction rates. On the other hand, intracellular reactions are also much faster than extracellular ones which allows considering the internal metabolites in a pseudo-steady state (Stephanopoulos et al., 1998). Eq. (1) therefore reduces to an homogeneous system of linear equations:

$$N\underline{\nu} = 0 \tag{2}$$

It is important to note that the dynamic behaviour of the system is not completely disregarded with the use of the latter assumption since extracellular dynamics can still be introduced in the system via the cellular uptake and production rates (Llaneras and Picó, 2008). Besides, to ensure that the reactions proceed in the appropriate direction, network fluxes are usually positively constrained:

$$\underline{\nu_i} > 0 \quad i = 1, \ldots, I \tag{3}$$

where I is the number of irreversible fluxes (or fluxes with direct contribution larger than their reverse counterpart).

In metabolic network analysis, the number of studied metabolites is usually much lower than the number of reactions considered in the network. Equation system (2) under the constraints (3) is thus usually underdetermined with $n - m$ degrees of freedom (DoF) and leads to an infinity of admissible solutions $\underline{\nu}$. The addition of m_e extracellular fluxes inferred from the measurements of the external compounds allows reducing the underdeterminacy of the system ($DoF = n - (m + m_e)$). These extracellular fluxes are linked to the network fluxes $\underline{\nu}$ via a matrix $N_e \in \Re^{m_e \times m}$:

$$\underline{\nu_e} = N_e\underline{\nu} \tag{4}$$

and the new system of equations can be written as:

$$\begin{pmatrix} N & 0 \\ N_e & -\underline{\nu_e} \end{pmatrix} \times \begin{pmatrix} \underline{\nu} \\ 1 \end{pmatrix} = 0 \tag{5}$$

2.1. Classical FVA approach

Even with the addition of these m_e new equations, system (5) often remains underdetermined. Nevertheless, the extreme values of the set of admissible fluxes $\underline{\nu}$ can be calculated using an FVA approach defined as follows (Mahadevan and Schilling, 2003; Llaneras and Picó, 2007; Richelle et al., 2016):

$$\forall t_k, \forall j = 1, \ldots, n \quad \begin{cases} \nu_{j,up}(t_k) = max\left(\nu_j(t_k)\right) \\ \nu_{j,low}(t_k) = min\left(\nu_j(t_k)\right) \end{cases} s.t. \begin{cases} N\underline{\nu}(t_k) = 0 \\ \underline{\nu}(t_k) \geq 0 \\ N_e\underline{\nu}(t_k) = \underline{\nu_e}(t_k) \end{cases} \tag{6}$$

The former system defines a series of 2n Linear Programs (LPs) where each flux ν_j $(j = 1, \ldots, n)$ is in turn minimized $\nu_{j,\,low}(t_k)$ and maximized $\nu_{j,up}(t_k)$. To take the measurement noise and the subsequent data-smoothing into account, a coefficient of variation

e_ν that defines the interval representation of fluxes can be introduced in the Eq. (6) so that the system is written under the form:

$$\forall t_k, \forall j = 1, \ldots, n$$
$$\begin{cases} \nu_{j,up}(t_k) = max\left(\nu_j(t_k)\right) \\ \nu_{j,low}(t_k) = min\left(\nu_j(t_k)\right) \end{cases} s.t. \begin{cases} N\underline{\nu}(t_k) = 0 \\ \underline{\nu}(t_k) \geq 0 \\ N_e\underline{\nu} \leq (1+e_\nu)\underline{\nu}_e(t_k) \\ N_e\underline{\nu} \geq (1-e_\nu)\underline{\nu}_e(t_k) \end{cases} \tag{7}$$

2.2. Adaptive flux variability analysis

In previous studies (Llaneras and Picó, 2007; Richelle et al., 2016; Bogaerts et al., 2017), the minimum value e_ν that leads to admissible solutions for LP (7) is determined incrementally, starting with a value of 0 and increasing it until the system admits solutions. The idea proposed in Abbate et al. (2019) is to consider the coefficient of variation e_ν as an unknown variable in the LP problem, and to calculate along time the minimum $e_\nu(t_k)$ that satisfies all the problem constraints:

$$\forall t_k, \quad e_{\nu,low}(t_k) = \min_{\underline{\nu}'(t_k)} \underline{\lambda}^T \underline{\nu}'(t_k)$$
$$s.t. \begin{cases} N\underline{\nu}(t_k) = 0 \\ \underline{\nu}'(t_k) \geq 0 \\ N'_{e-}\underline{\nu}'(t_k) \leq \underline{\nu}_e(t_k) \\ N'_{e+}\underline{\nu}'(t_k) \geq \underline{\nu}_e(t_k) \end{cases} \quad with \quad \begin{aligned} \underline{\nu}'(t_k) &= \begin{bmatrix} \underline{\nu}(t_k) \\ e_\nu(t_k) \end{bmatrix} \\ N'_{e-}(t_k) &= \begin{bmatrix} N_e & -\underline{\nu}_e(t_k) \end{bmatrix} \\ N'_{e+}(t_k) &= \begin{bmatrix} N_e & \underline{\nu}_e(t_k) \end{bmatrix} \\ \underline{\lambda}^T &= \begin{bmatrix} \underline{0}_{1,n} & 1 \end{bmatrix} \end{aligned} \tag{8}$$

where $\underline{\nu}'(t_k) \in \Re^{(n+1)}$, $N'_{e+}(t_k)$ as well as $N'_{e-}(t_k) \in \Re^{(m_e,n+1)}$, and $\underline{0}_{1,n}$ is a row vector with n zeros. Once the time dependent coefficients of variation $e_\nu(t_k)$ are obtained, they can be introduced in LP (7) to obtain the narrowest admissible set of solutions. Note that this method might lead to somewhat large coefficients of variation, in which case, the user might need to reconsider either the data smoothing and/or the suitability of the network to describe the specific experimental data.

The advantage of the adaptive flux variability analysis is that the relaxation of constraints, which allows LP (7) to have admissible solutions, is not constant over time and ensures the smallest internal flux intervals.

Adaptive flux variability analysis can also be extended to the case where coefficients of variation are different for each considered external flux. In this case, LP (8) becomes:

$$\forall t_k, \left\|\underline{e}_{\nu,low}(t_k)\right\|_1 = \min_{\underline{\nu}''(t_k)} \underline{\lambda}^T \underline{\nu}''(t_k)$$
$$s.t. \begin{cases} N\underline{\nu}(t_k) = 0 \\ \underline{\nu}''(t_k) \geq 0 \\ N''_{e-}\underline{\nu}'' \leq \underline{\nu}_e(t_k) \\ N''_{e+}\underline{\nu}'' \geq \underline{\nu}_e(t_k) \end{cases} \quad with: \quad \begin{aligned} \underline{\nu}''(t_k) &= \begin{bmatrix} \underline{\nu}(t_k) \\ \underline{e}_\nu(t_k) \end{bmatrix} \\ N''_{e-}(t_k) &= \begin{bmatrix} N_e & -V_e(t_k) \end{bmatrix} \\ N''_{e+}(t_k) &= \begin{bmatrix} N_e & V_e(t_k) \end{bmatrix} \\ \underline{\lambda}^T &= \begin{bmatrix} \underline{0}_{1,n} & \underline{1}_{1,m_e} \end{bmatrix} \end{aligned} \tag{9}$$

where $\underline{e}_\nu(t_k) \in \Re^{m_e}$ is a column vector containing the coefficients of variation relative to the external flux vector $\underline{\nu}_e$, $\underline{\nu}''(t_k) \in \Re^{(n+m_e)}$, $N''_{e-}(t_k)$ and $N''_{e+}(t_k) \in \Re^{(m_e,n+m_e)}$, $\underline{0}_{1,n}$ is a row vector with n zeros, $\underline{1}_{1,m_e}$ is a row vector with m_e elements equal to 1, while $V_e(t_k) \in \Re^{(m_e \times m_e)}$ is a diagonal matrix in which elements $V_{e,jj}(t_k)$ $j = (1, \ldots, m_e)$ are the corresponding external fluxes, namely $\nu_{e,j}(t_k)$.

2.3. Absolute and normalized coefficients of variation

In Eq. (9), the coefficients of variation are introduced to model relative errors with respect to the observed fluxes $\nu_e(t_k)$ at each time of analysis t_k. Yet, since external fluxes may significantly vary along the culture, coefficients of variation might evolve accordingly, ranging from very small in the case of large fluxes to very large when these fluxes tend to zero. In consequence, a slight perturbation of a small flux might have a significant impact on the optimization problem 9.

In order to tackle this issue, the nature of the considered errors should be changed. One possibility is to consider absolute errors. In this case, Eq. (7) becomes:

$$\forall t_k, \forall j = 1, \ldots, n$$
$$\begin{cases} \nu_{j,up}(t_k) = max\left(\nu_j(t_k)\right) \\ \nu_{j,low}(t_k) = min\left(\nu_j(t_k)\right) \end{cases} s.t. \begin{cases} N\underline{\nu}(t_k) = 0 \\ \underline{\nu}(t_k) \geq 0 \\ N_e\underline{\nu} \leq \underline{\nu}_e(t_k) + e_\nu(t_k) \\ N_e\underline{\nu} \geq \underline{\nu}_e(t_k) - e_\nu(t_k) \end{cases} \tag{10}$$

This type of errors will however give the prevalence to large fluxes in the optimization problem, possibly leading to distortion or abrupt changes in the smallest fluxes.

Another solution is to normalize the coefficients of variation and to rewrite Eq. (7) under the form:

$$\forall t_k, \forall j = 1, \ldots, n$$
$$\begin{cases} \nu_{j,up}(t_k) = max\left(\nu_j(t_k)\right) \\ \nu_{j,low}(t_k) = min\left(\nu_j(t_k)\right) \end{cases} s.t. \begin{cases} N\underline{\nu}(t_k) = 0 \\ \underline{\nu}(t_k) \geq 0 \\ N_e\underline{\nu} \leq \underline{\nu}_e(t_k) + e_\nu(t_k) max(\underline{\nu}_e) \\ N_e\underline{\nu} \geq \underline{\nu}_e(t_k) - e_\nu(t_k) max(\underline{\nu}_e) \end{cases} \tag{11}$$

The use of normalized errors allows distributing the uncertainties more evenly on each signals, independently of their magnitudes.

These three types of error representations are discussed in Section 4.

2.4. Calculation of the external fluxes

The m_e external fluxes, which constrain the optimization problem, are inferred from the extracellular concentration measurements. Indeed, these fluxes are the specific consumption/production rates of the measured culture substrates and products, respectively. They can be easily isolated in the equations of the general state space model of a perfused cell culture:

$$\begin{aligned} \dot{X} &= \nu_X X - (1-\alpha)DX - k_d X \\ \dot{\underline{S}} &= -\underline{\nu}_S X + D(\underline{S}_{in} - \underline{S}) \\ \dot{\underline{P}} &= \underline{\nu}_P X + D(\underline{P}_{in} - \underline{P}) \\ \dot{V} &= 0 \end{aligned} \tag{12}$$

where X is the viable biomass in $10^9 cells/l$, $\underline{S}$ and $\underline{P}$ are respectively the substrate and product concentration vectors (in $mmol/l$), D is the dilution rate (h^{-1}) that feeds the culture, α is the retention factor ($\alpha = 1$ corresponds to complete retention), V is the constant bioreactor volume (l), ν_X is the specific growth rate in h^{-1}, k_d is the specific mortality rate in h^{-1}, and $\underline{\nu}_j$ $(j = S, P)$ are the specific consumption/uptake rates expressed in $mmol.(h.10^9 cells)^{-1}$. The left hand-side time derivatives of system (12) are simply replaced by the derivatives of the smoothing-splines applied to the concentration measurements (this can be achieved in the Matlab environment using the functions *spaps* for smoothing and *fnder* for differentiation).

2.5. Materials and methods

HEK-293 cell cultures were conducted in an *ambr® 250 high throughput (Sartorius)* automated bioreactor system. The latter allows 24 parallel runs of 100–250 ml disposable bioreactors. Runs

are performed in duplicates or triplicates and consist in simple batches with glucose adjustments. The data used in this study originates from one run of a triplicate.

Biomass and viability are assessed using a *Vi-Cell* ™ *device (Beckman Coulter)* that performs the trypan blue dye exclusion method.

Glucose, lactate, glutamate, ammonium ions and pyruvate are measured using a *Cedex Bio HT Analyzer (Roche Custom Biotech)*.

Amino acids are quantified using UPLC measurements *(Waters)* through derivatization, separation in a simple column and UV detection.

Urea is measured through quantitative colorimetric assays (BioChain®).

For the sake of confidentiality, relatively little detail about the culture conditions can be provided. pH is controlled at 7,2 while temperature is maintained at 37 °C.

The smoothing splines based on the experimental data are shown in Fig. 1. Three different types of smoothing have been considered to draw these graphs:

1. Soft: splines embrace all measurement points (yellow curves)
2. Medium: splines qualitatively fit the data (blue curves)
3. Strong: splines using smoothing weights 10 times larger than in the medium smoothing (red curves)

It is interesting to note that even if the concentration splines look similar, their derivatives and in turn, the inferred values of the fluxes may be quite different. The impact of smoothing on the results is discussed in Section 4.2.

3. Network presentation

The network used in this work has been largely inspired from Fernandes et al. (2016) and adapted to take all available measurements into account. It contains $r = 82$ reactions among which 27 are transport reactions, $m = 51$ internal metabolites and $p = 27$ external metabolites measured in the extracellular medium (CO_2 is not measured), and is presented in Table 1. It encompasses the main metabolic pathways, namely the glycolysis, pentose phosphate pathway, Tricarboxylic Acid Cycle (TCA), a couple of anaplerotic reactions, several reactions of the amino acid metabolism and the urea cycle.

It also contains two reactions for the biomass synthesis, namely one reaction for the nucleotide synthesis and another for the biomass itself. It must be stressed that although Table 1 includes the reaction cofactors such as NAD^+, *NADH, ATP, ADP, AMP,* ...the latter are not considered in the network. Also, even though Table 1 includes all potential reversible reactions, only four of them are actually allowed proceeding in both directions : ν_{15}, ν_{16}, ν_{45} and ν_{47}, which are necessary to describe the dynamics observed in the datasets regarding Ala, Lac, Orn and Asn. The direction of the other reactions is fixed from left to right in Table 1. Since animal cells are not able to synthesize all 20 amino acids, essential amino acids (Met, His, Thr, Arg, Ile, Leu, Val, His, Phe, Trp) can only be consumed, while non-essential amino-acids and pyruvate can go in and out of the cell. Besides, urea can only be produced.

The biomass synthesis reaction is also borrowed from the metabolic network of Fernandes et al. (2016) which is designed for CHO cells, and not HEK cells. Nevertheless, Pe'er et al. (2004) proves that the average amino acid composition of eukaryote cells is very similar from one strain to another. It is therefore assumed that the former synthesis reaction can be used to model the related biomass flux.

4. Results and discussion

4.1. FVA and AVFA comparison and effect of the formulation of the coefficients of variation

The original FVA approach (Llaneras and Picó, 2007; Richelle et al., 2016; Bogaerts et al., 2017) is first applied to the considered metabolic network and datasets. In this analysis (denoted A1), only one coefficient of variation is identified, which is constant over time and common to all the variables. On the other hand, analysis A2 is based on the proposed AFVA methodology, so that the coefficients of variation are allowed varying along the course of the experiments, but remain common to all the variables. Finally, analysis A3 is performed using time- and variable-dependent coefficients of variation. Solutions are calculated every 5h of the experiment time-course for each analysis and using the medium smoothing-splines (blue curves of Fig. 1). The three analyses are performed in the *Matlab* environment using the *dual-simplex* algorithm implemented in the *linprog* function, which appears to be the fastest among all the available algorithms. Nevertheless, when the number of variables increases, numerical issues may arise. In this case, the coefficients of variation (of analysis A3) are first identified using an *interior-point* algorithm, and further refined using the dual-simplex algorithm. Moreover, once identified, the smallest coefficients of variation are slightly increased (arbitrarily by 2%) to prevent further numerical issues.

The analyses are performed for each type of errors, namely relative, absolute and normalized. The inferred internal fluxes using a relative error model are shown in Fig. 2a while Figs. 3a and 4a present the results obtained using absolute and normalized errors, respectively. As observed in Abbate et al. (2019), the intervals obtained in analysis A1 (blue areas) are always the largest and encompass those of analysis A2 (red areas). The latter observation is obvious since at each time step, the identified coefficient of variation is always lower or equal to the one used in analysis A1, and therefore constitutes an upper limit of the studied solution in A2. The intervals obtained in analysis A3 (upper and lower limits in green) are clearly smaller, upper and lower limits being even often indistinguishable, and most of the time within A2 intervals. However, it can be noticed that some fluxes inferred using the absolute error model (ν_{33}) or normalized error model (ν_{24}, ν_{28} and ν_{29}) slightly go over the A1 upper bounds. This is due to the variable-dependent distribution of the error in A3 conversely to A1 and A2 where the errors are equal for all species.

Moreover, the inferred internal fluxes of analyses A1 and A2 present different shapes depending on the error nature. Globally, it can be noticed that relative coefficients of variation induce larger intervals (Fig. 2a) at the beginning of the experiment than absolute and normalized coefficients (Figs. 3a and 2a respectively). In contrast, it seems that relative coefficients of variation provide the smallest intervals in A1 and A2 at the end of the experiment, while those of A2 are larger on average. However, the fluxes encompassed in the glycolysis, pentose phosphate pathway, and TCA cycle are more accurate in A2, as compared to the optimal solutions of A3.

It is also observed that flux ν_{16} calculated in A3 with a relative error model displays a strange discontinuous shape. Indeed, this flux reverses back and forth many times along the course of the experiment when using relative coefficient of variations. Yet, this flux is directly linked to the external entry/exit of alanine, and this behaviour is not observed with the other error models.

As a validation of the analysis, the estimated fluxes are integrated to evaluate the evolution of the concentrations, which can then be compared to the original smoothing curves in Figs. 2b, 3b and 4b. The concentration intervals of the classical FVA (A1 - blue curves) are wide and often include negative values, which is

Table 1
HEK cell metabolic network considered in the AVFA analyses.

	Metabolic Reaction network
	Glycolysis
v_1	$Glc + ATP \rightarrow G6P + ADP$
v_2	$G6P \leftrightarrow F6P$
v_3	$F6P + ATP \rightarrow DHAP + G3P + ADP$
v_4	$DHAP \leftrightarrow G3P$
v_5	$G3P + NAD^+ + ADP \leftrightarrow 3PG + NADH + ATP$
v_6	$3PG + ADP \rightarrow Pyr + ATP$
	Tricarboxylic Acid Cycle
v_7	$Pyr + NAD^+ + CoASH \rightarrow AcCoA + CO_2 + NADH$
v_8	$AcCoA + Oxal + H_2O \rightarrow Cit + CoASH$
v_9	$Cit + NAD(P)^+ \rightarrow \alpha KG + CO_2 + NAD(P)H$
v_{10}	$\alpha KG + CoASH + NAD^+ \rightarrow SucCoA + CO_2 + NADH$
v_{11}	$SucCoA + GDP + Pi \leftrightarrow Succ + GTP + CoASH$
v_{12}	$Succ + FAD \leftrightarrow Fum + FADH_2$
v_{13}	$Fum \leftrightarrow Mal$
v_{14}	$Mal + NAD^+ \leftrightarrow Oxal + NADH$
	Pyruvate Fates
v_{15}	$Pyr + NADH \leftrightarrow Lac + NAD^+$
v_{16}	$Pyr + Glu \leftrightarrow Ala + \alpha KG$
	Pentose Phosphate Pathway
v_{17}	$G6P + 2NADP^+ + H_2O \rightarrow R5P + 2NADPH + CO_2$
v_{18}	$G6P + 2NADP^+ + H_2O \rightarrow X5P + 2NADPH + CO_2$
v_{19}	$2X5P + R5P \leftrightarrow 2F6P + G3P$
	Anaplerotic Reaction
v_{20}	$Mal + NAD(P)^+ \leftrightarrow Pyr + CO_2 + NAD(P)H$
v_{21}	$Pyr + CO2 + ATP \leftrightarrow Oxal$
	Amino Acid Metabolism
v_{22}	$Glu + NAD(P)^+ \leftrightarrow \alpha KG + NH_4^+ + NAD(P)H$
v_{23}	$Oxal + Glu \leftrightarrow Asp + \alpha KG$
v_{24}	$Gln \rightarrow Glu + NH_4^+$
v_{25}	$Thr + NAD^+ + CoASH \rightarrow Gly + NADH + AcCoA$
v_{26}	$Ser \leftrightarrow Gly$
v_{27}	$3PG + Glu + NAD^+ \rightarrow Ser + \alpha KG + NADH$
v_{28}	$Gly + NAD^+ \rightarrow CO_2 + NH_4^+ + NADH$
v_{29}	$Ser \rightarrow Pyr + NH_4^+$
v_{30}	$Thr \rightarrow \alpha Kb + CoASH + NAD^+ + NH_4^+$
v_{31}	$\alpha Kb + CoASH + NAD^+ \rightarrow PropCoA + NADH + CO_2$
v_{32}	$PropCoA + HCO_3^- + ATP \rightarrow SucCoA + ADP + Pi$
v_{33}	$Lys + 2\alpha KG + 3NAD(P) + FAD^+ \rightarrow \alpha Ka + 2Glu + 3NAPH + FADH_2$
v_{34}	$Trp \rightarrow Ala + 2CO_2 + \alpha Ka$
v_{35}	$\alpha Ka + CoASH + 2NAD^+ \rightarrow AcetoAcCoA + 2NADH + 2CO_2$
v_{36}	$AcetoAcCoA + CoASH \rightarrow 2AcCoA$
v_{37}	$Val + \alpha KG + CoASH + 3NAD^+ + FAD^+ \rightarrow PropCoA + Glu + 2CO_2 + 3NADH + FADH_2$
v_{38}	$Ile + \alpha KG + 2CoASH + 2NAD^+ + FAD^+ \rightarrow AcCoA + PropCoA + Glu + CO_2 + 2NADH + FADH_2$
v_{39}	$leu + \alpha KG + CoASH + NAD^+ + FAD^+ + HCO_3^- + ATP \rightarrow AcCoA + AcetoAc + Glu + CO_2 + NADH + FADH_2$
v_{40}	$AcetoAc + SucCoA \rightarrow AcetoAcCoA + Succ$
v_{41}	$Phe + NADH \rightarrow Tyr + NAD^+$
v_{42}	$Tyr + \alpha KG \rightarrow Fum + AcetoAc + Glu + CO_2$
v_{43}	$Met + Ser + ATP \rightarrow Cys + \alpha Kb + NH_4^+ + AMP$
v_{44}	$Cys \rightarrow Pyr + NH_4^+$
v_{45}	$Asn \leftrightarrow Asp + NH_4^+$
v_{46}	$Orn + \alpha KG \leftrightarrow Glu_\gamma SA + Glu$
v_{47}	$Glu + ATP + 2NADPH + H^+ \leftrightarrow Pro + ADP + 2NADP^+$
v_{48}	$Glu_\gamma SA \leftrightarrow Pro-$
v_{49}	$His \rightarrow Glu + NH_4^+$
	Urea Cycle
v_{50}	$Arg \rightarrow Orn + urea$
v_{51}	$NH_4^+ + CO_2 + 2ATP + Orn \rightarrow Cln$
v_{52}	$Cln + Asp + ATP \rightarrow ArgSucc + AMP$
v_{53}	$ArgSucc \rightarrow Arg + Fum$
	Nucleotides synthesis
v_{54}	$2Asp + 1Gly + 2Gln + 0.6R5P + CO2 \rightarrow 2Mal + 2Glu$
	Biomass synthesis
v_{55}	$0.024R5P + 0.029G6P + 0.04Gln + 0.013Ala + 0.007Arg + 0.026Asp + 0.003His + 0.0084Ile + 0.013Leu + 0.01Lys + 0.099Ser + 0.004Tyr + 0.0096Val + 0.016Gly + 3.78ATP \rightarrow Biomass$
	Transport Reactions
v_{56}	$Glc_{ext} \rightarrow Glc$
v_{57}	$Gln_{ext} \rightarrow Gln$
v_{58}	$Lac \rightarrow Lac_{ext}$
v_{59}	$NH_4^+ \rightarrow NH_{4\ ext}^+$
v_{60}	$Ala \rightarrow Ala_{ext}$
v_{61}	$Asp_{ext} \rightarrow Asp$
v_{62}	$Asn_{ext} \rightarrow Asn$
v_{63}	$Glu \rightarrow Glu_{ext}$

(*continued on next page*)

Table 1 (*continued*)

	Metabolic Reaction network
v_{64}	$Ser_{ext} \rightarrow Ser$
v_{65}	$Arg_{ext} \rightarrow Arg$
v_{66}	$Gly \rightarrow Gly_{ext}$
v_{67}	$Pro_{ext} \rightarrow Pro$
v_{68}	$Tyr_{ext} \rightarrow Tyr$
v_{69}	$His_{ext} \rightarrow His$
v_{70}	$Ile_{ext} \rightarrow Ile$
v_{71}	$Leu_{ext} \rightarrow Leu$
v_{72}	$Lys_{ext} \rightarrow Lys$
v_{73}	$Met_{ext} \rightarrow Met$
v_{74}	$Phe_{ext} \rightarrow Phe$
v_{75}	$Thr_{ext} \rightarrow Thr$
v_{76}	$Val_{ext} \rightarrow Val$
v_{77}	$CO_2 \rightarrow CO_{2,ext}$
v_{78}	$Cys_{ext} \rightarrow Cys$
v_{79}	$Orn \rightarrow Orn_{ext}$
v_{80}	$Urea \rightarrow Urea_{ext}$
v_{81}	$Pyr \rightarrow Pyr_{ext}$
v_{82}	$Trp_{ext} \rightarrow Trp$

physically not possible. This emphasizes that a part of the internal fluxes obtained using the classical FVA method should be rejected in order to avoid such non-admissible negative concentrations. Unfortunately, it is impossible to discriminate admissible and non-admissible fluxes among the solutions.

On the contrary, concentrations obtained using analysis A3 are precisely defined, with equal lower and upper limits. Most of the estimated fluxes are very close to the initial smoothing-splines. It must be noted however that some metabolite concentrations are not well reproduced, especially the concentrations of NH3 and Arg when normalized coefficient of variation are used (Fig. 4b), and Ala, Ser and Arg when the coefficients of variation are relative. The wrong estimations of Ala in the latter case is directly linked to the strange behaviour of v_{16}. Interestingly, the integration of the internal fluxes obtained using absolute errors faithfully reproduce the data.

These results confirm the interest of using AFVA, as compared to the classical FVA approach. The quality of the reconstructed concentrations is quite remarkable even using an approximative description of the biomass reaction and supports the observation of Pe'er et al. (2004) which suggests that the average amino acid composition of eukaryote cells is very similar from one strain to another.

In a last round of tests, the possibility to relax the constraints with different amplitudes for the upper and lower bounds of the intervals is investigated (i.e., the consideration of non-centred intervals). This could be useful in analyses A1 or A2, since a single coefficient of variation is estimated for all the external metabolite fluxes, but has no relevance in analysis A3, since coefficients of variation are determined for each individual external flux and already provide either an upper or lower bound relaxation. These results are not shown in this article for the sake of brevity, as A3 remains the best performing and recommended approach.

4.2. Influence of data smoothing

The potential effect of data-smoothing is studied by performing AFVA using normalized coefficients of variation (Analysis A3) and for the three different intensity of smoothing previously defined. The results are compared in Fig. 5 and show the mild impact of data-smoothing on the quality of the estimated flux intervals. Indeed, except for some variations in v_{33}, v_{34}, v_{38}, v_{41}, ..., most of the flux ranges remain unaltered. These results confirm the robustness of AFVA. As a general recommendation, the use of a strong smoothing is therefore advisable.

4.3. Taking advantage of AFVA to fix biomass production rates

Imposing the biomass production rate as a measured external signal might lead to system infeasibility since it constitutes a stringent constraint alongside with other measured fluxes. Yet, when this flux is not imposed, the resulting interval for the biomass production rate can be quite large (see blue areas of flux v_{55} in Figs. 2a, 3a and 4a). AFVA offers the possibility to fix the biomass growth rate and to study the resulting internal flux distribution. This section compares the AFVA results with those obtained using FBA, maximizing biomass production.

The viable biomass specific growth rate can be obtained from the corresponding mass balance Eq. (12) with $D = 0$ (batch operation):

$$\nu_X(t) = (\dot{X} + \dot{X}_d)/X = \dot{X}/X + k_d \tag{13}$$

where k_d is the specific death rate (cell lysis is assumed to be negligible). The viable biomass specific rate can be estimated from the measurements of the viable biomass concentration $X(t)$ and of the viability ratio $V_X = X/X_{tot}$, X_{tot} being the total biomass population (which is not directly measured). The total biomass and dead biomass populations can be estimated on the basis of the following expressions:

$$X_{tot} = X/V_X \qquad X_d = X_{tot}.(1 - V_X) \tag{14}$$

The dead cell dynamics $\dot{X}_d$ can be obtained by smoothing the measured signals and computing the time derivative.

The comparison between AFVA (analysis A3 without imposed biomass flux), FBA and AFVA+B (analysis A3 with biomass flux imposed), all performed using normalized coefficients of variation, is presented in Fig. 6. The FBA analysis is actually performed as an AFVA to ensure admissible solutions at each time of analysis. The maximum flux v_{55} of AFVA is then imposed to make sure that the biomass is always maximized as in a classic FBA. Maximum biomass fluxes v_{55} of AFVA and FBA are therefore superimposed in Fig. 6 and the maximum blue curve is thus not visible. Other flux intervals are then calculated. Qualitatively, it can be noticed that intervals computed with AFVA+B have a smoother evolution than with FBA. Interestingly, the maximum growth rate evaluated with AFVA+B is equal to $0.017h^{-1}$ while the one obtained with FBA is $0.052h^{-1}$, whereas a standard value in macro-modelling is $\approx 0.03h^{-1}$.

The same analysis, performed using absolute coefficients of variation, leads to the same observations. However, as shown in Fig. 7, the integration of the external fluxes leads to concentration

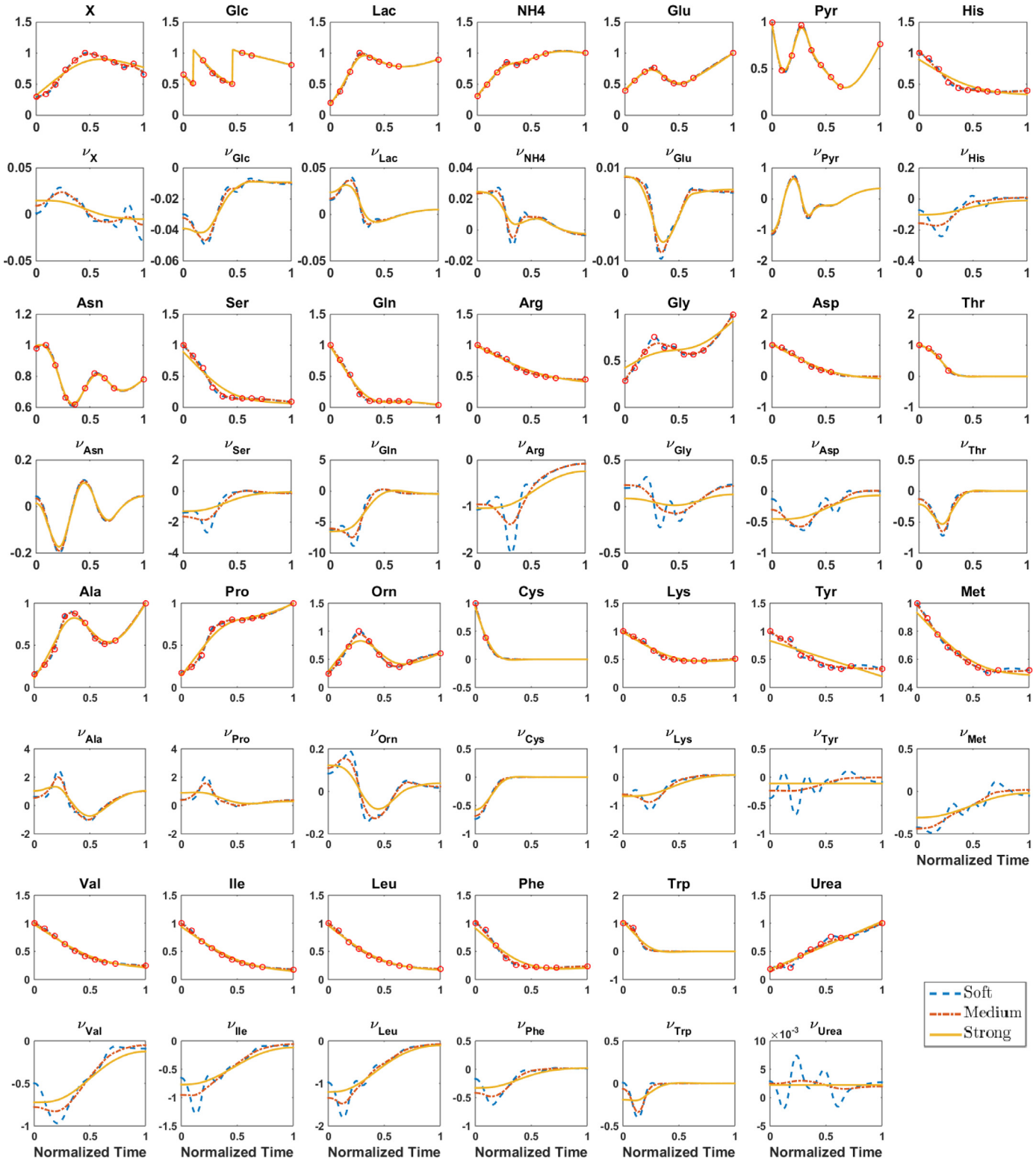

Fig. 1. Normalized concentration curves and inferred specific fluxes in $mmol.h^{-1}$ obtained for different types of smoothing (soft = blue curves, medium = red curves, strong = yellow curves). (For interpretation of the references to colour in this figure legend, the reader is referred to the web version of this article.)

signals which are not in agreement with the original splines and very different from those observed without imposing the biomass flux (Fig. 7a). This type of abnormalities is expected when solving optimization problems with signals of quite different magnitudes as discussed in Section 2.3. In contrast, the concentrations obtained using normalized coefficient of variations are in total agreement with former analyses (Fig. 7b). These results confirm that normalized coefficient of variations robustify AFVA.

In order to check the validity of these results, the biomass signals can be compared to living cells and viability measurements (Fig. 8). Indeed, the integration of the biomass growth rates obtained with FBA and AFVA+B provides the evolution of the total

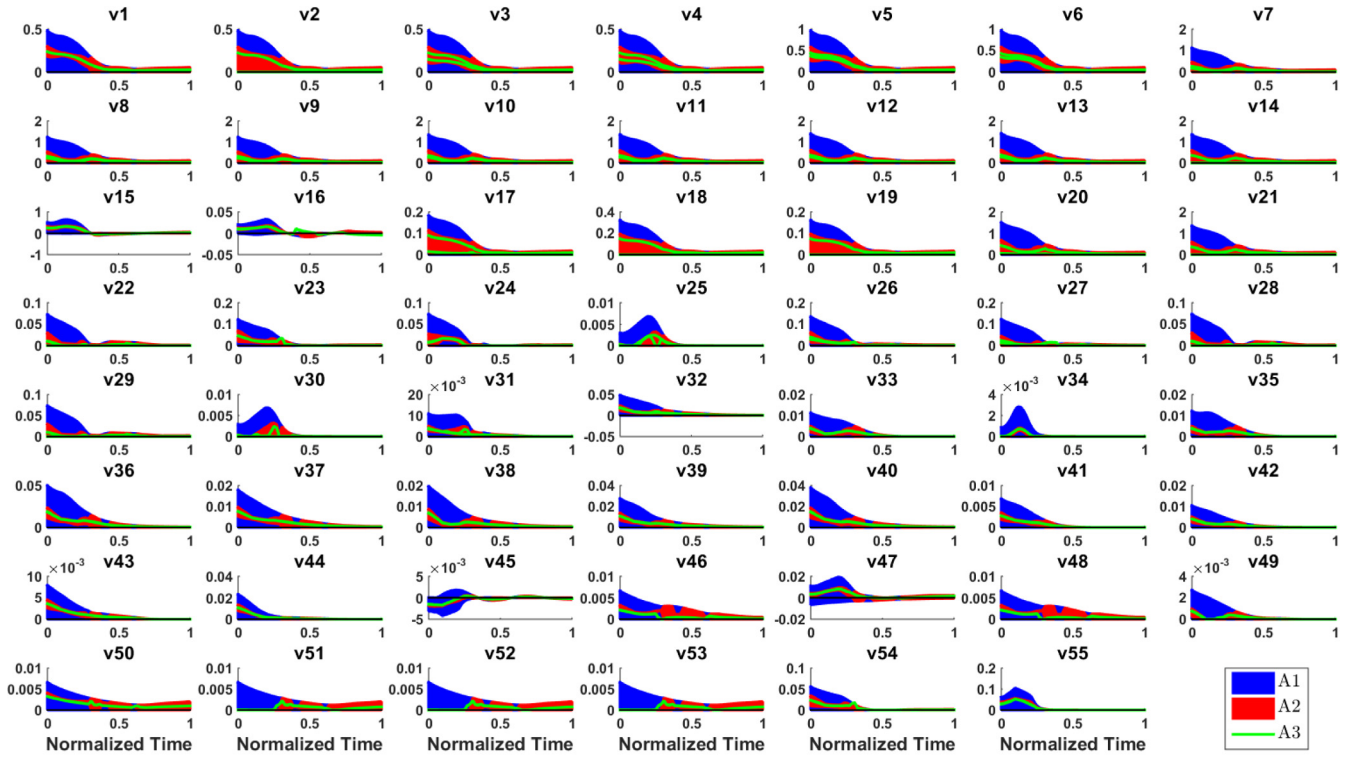

(a)

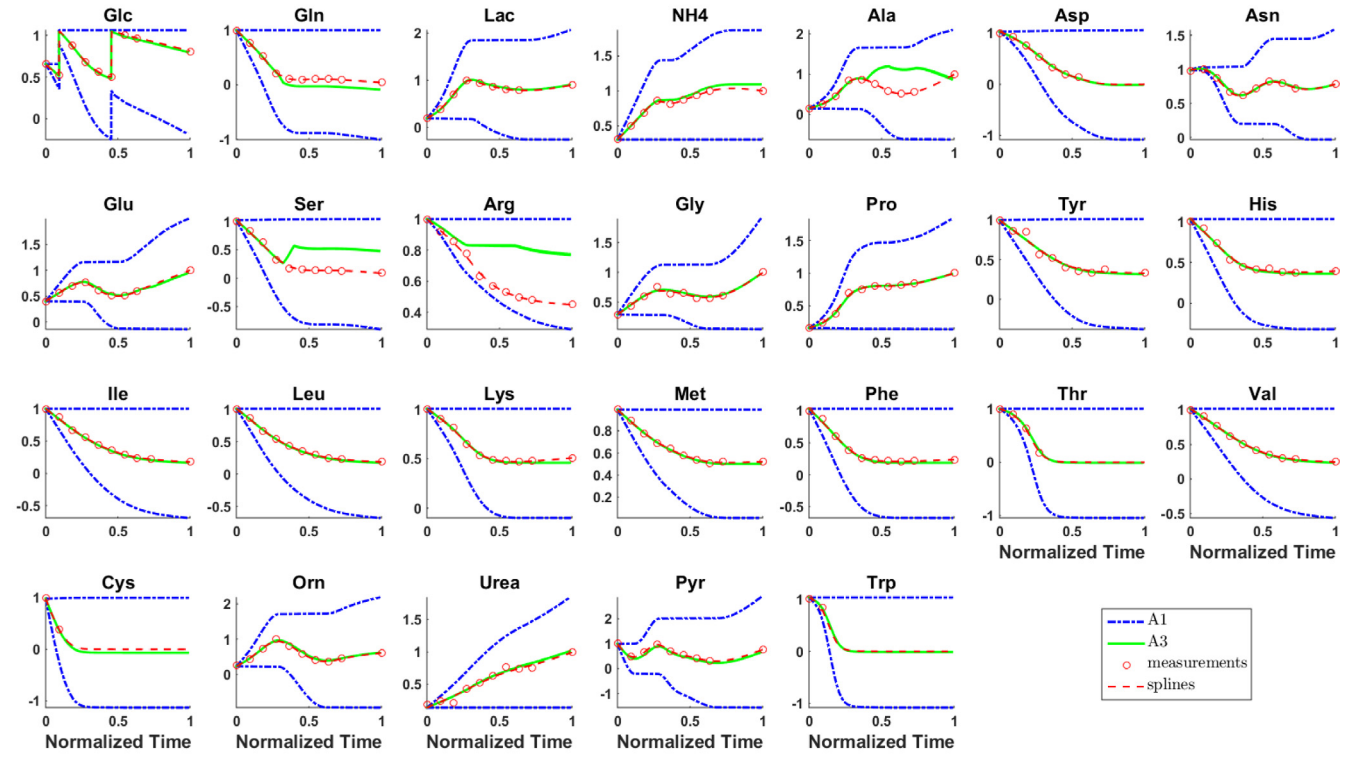

(b)

Fig. 2. Results using relative coefficients of variation: (a) Internal fluxes in $mmol.h^{-1}$ inferred from A1 (blue areas), A2 (red areas) and A3 (green curves); (b) Normalized external metabolite concentrations obtained through integration of the estimated flux intervals of A1 (blue curves) and A3 (green curves) compared to original splines (red dashed curves). (For interpretation of the references to colour in this figure legend, the reader is referred to the web version of this article.)

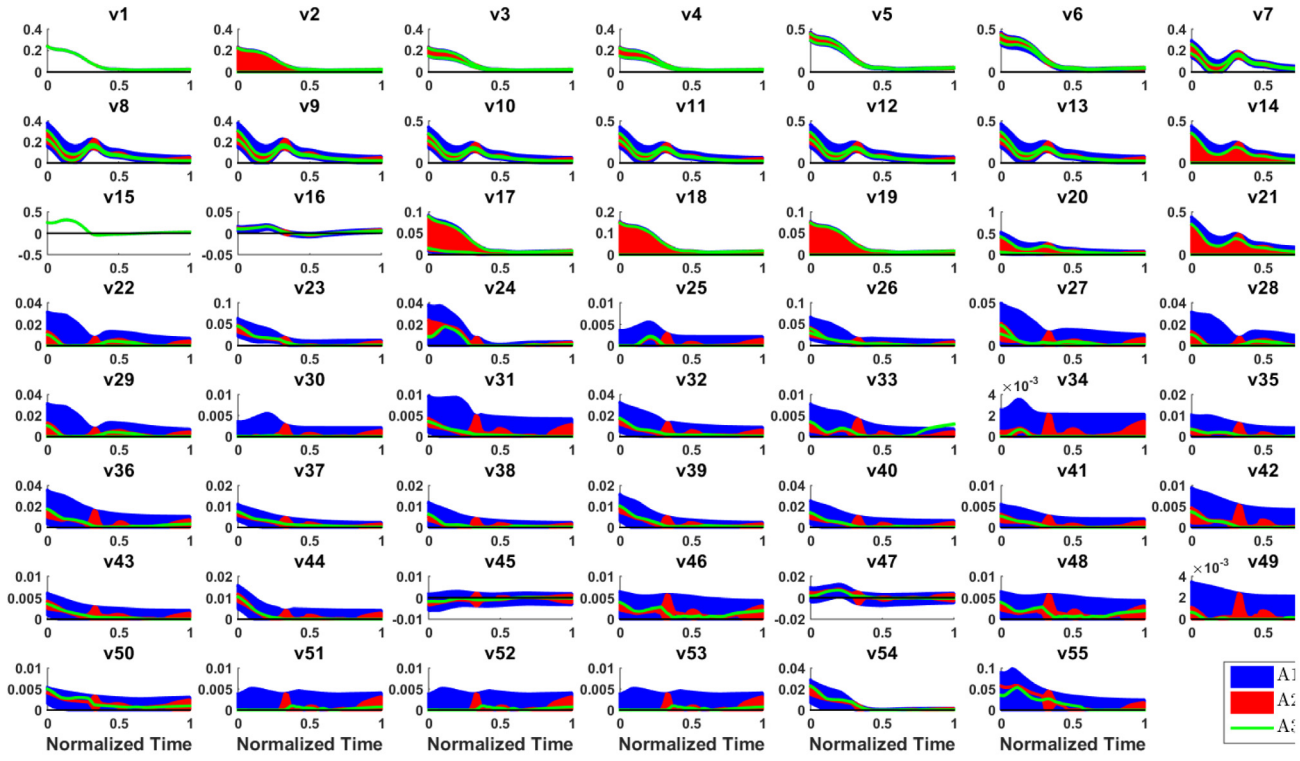

(a)

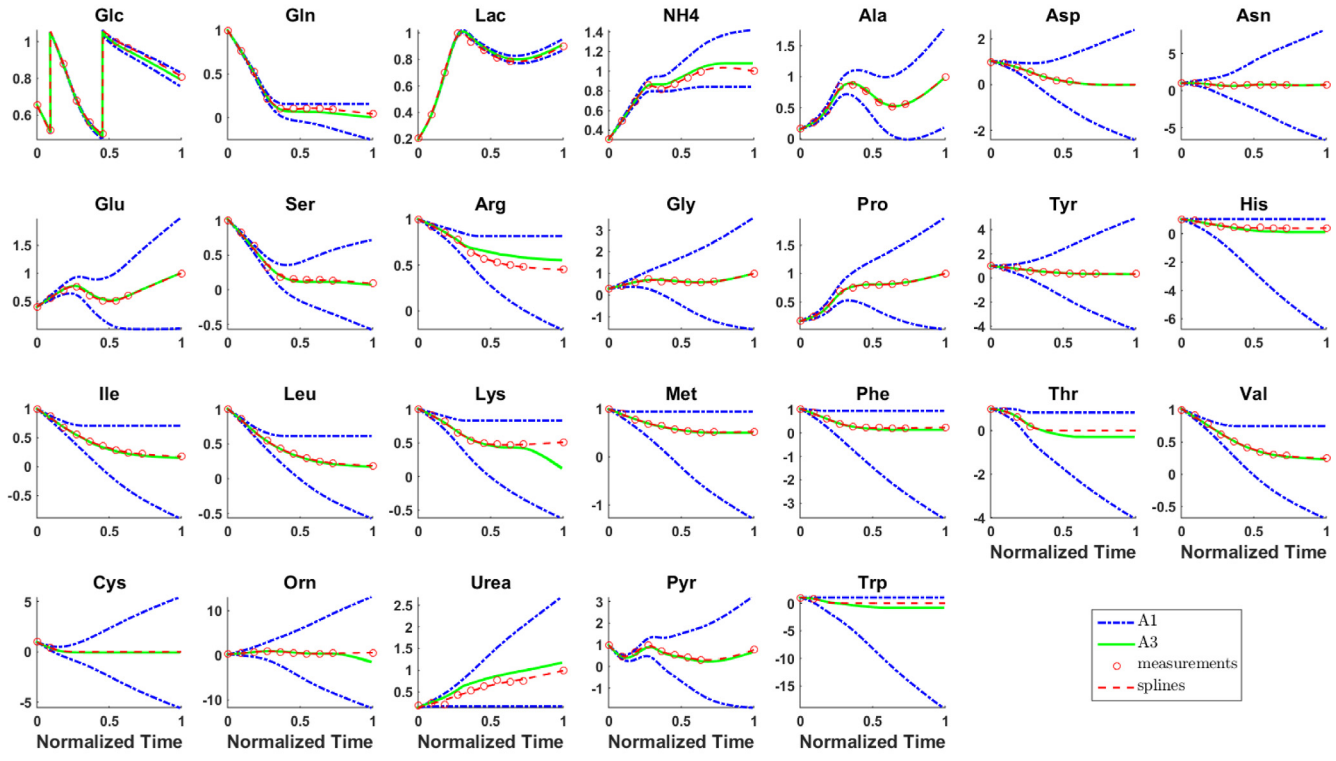

(b)

Fig. 3. Results using absolute coefficients of variation: (a) Internal fluxes in $mmol.h^{-1}$ inferred from A1 (blue areas), A2 (red areas) and A3 (green curves); (b) Normalized external metabolite concentrations obtained through integration of the estimated flux intervals of A1 (blue curves) and A3 (green curves) compared to original splines (red dashed curves). (For interpretation of the references to colour in this figure legend, the reader is referred to the web version of this article.)

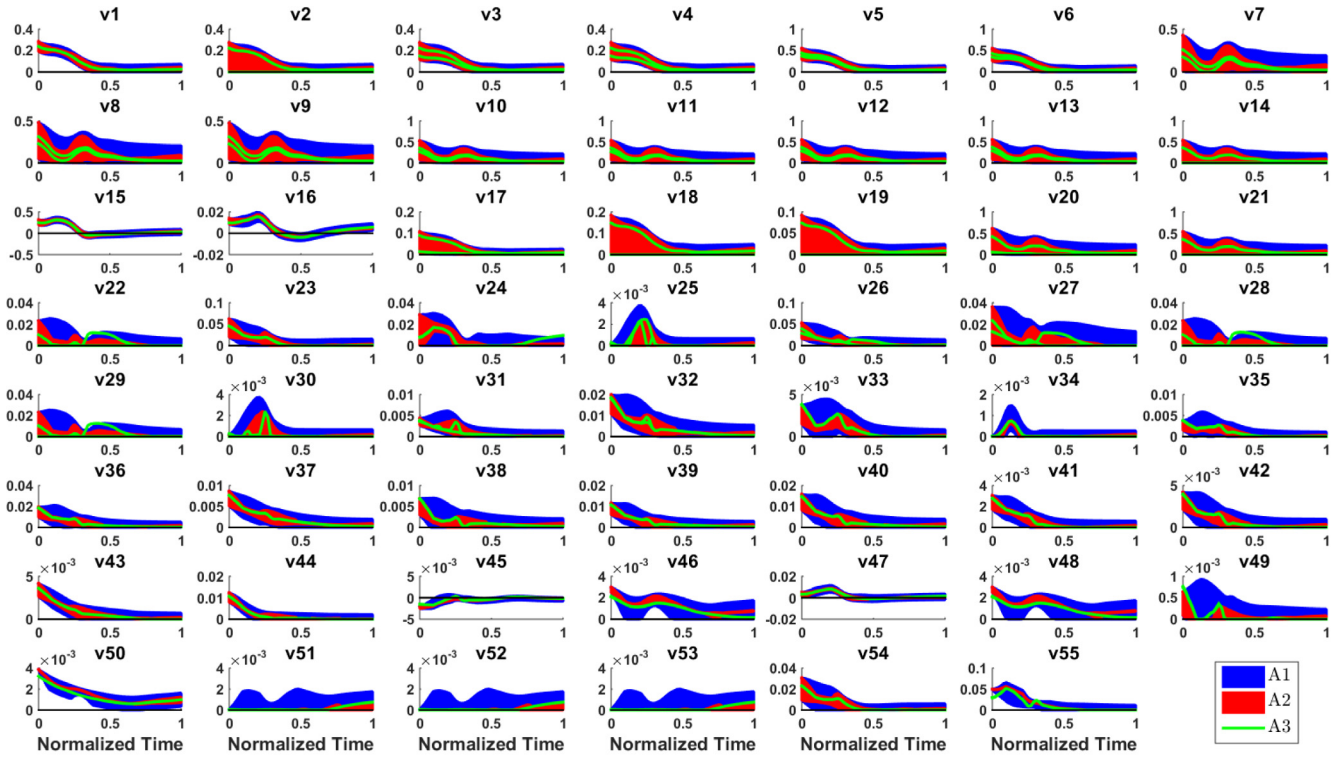

(a)

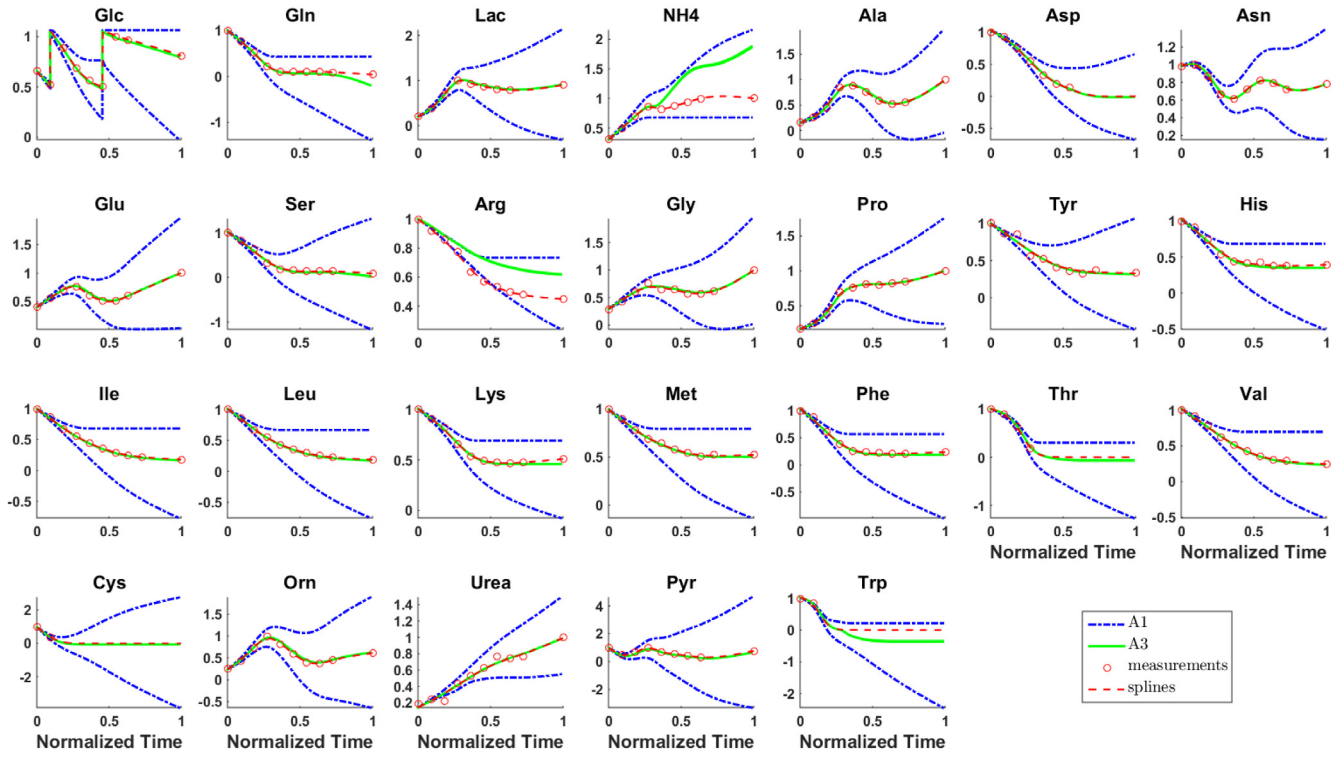

(b)

Fig. 4. Results using normalized coefficients of variation: (a) Internal fluxes in $mmol.h^{-1}$ inferred from A1 (blue areas), A2 (red areas) and A3 (green curves); (b) Normalized external metabolite concentrations obtained through integration of the estimated flux intervals of A1 (blue curves) and A3 (green curves) compared to original splines (red dashed curves). (For interpretation of the references to colour in this figure legend, the reader is referred to the web version of this article.)

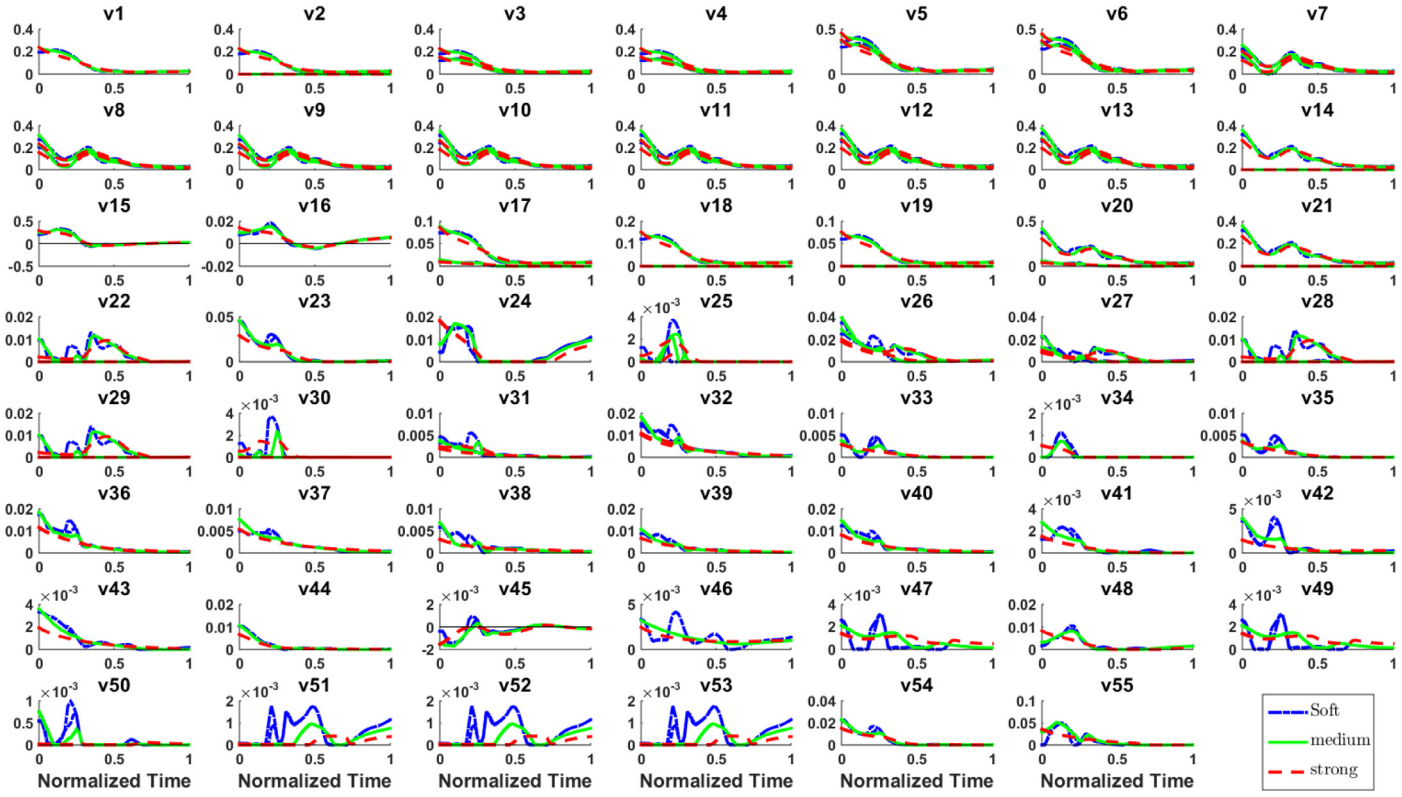

Fig. 5. Comparison of the internal fluxes obtained applying AFVA with different smoothing-splines (Soft smoothing = blue curves, medium smoothing = green curves, strong smoothing = red curves). (For interpretation of the references to colour in this figure legend, the reader is referred to the web version of this article.)

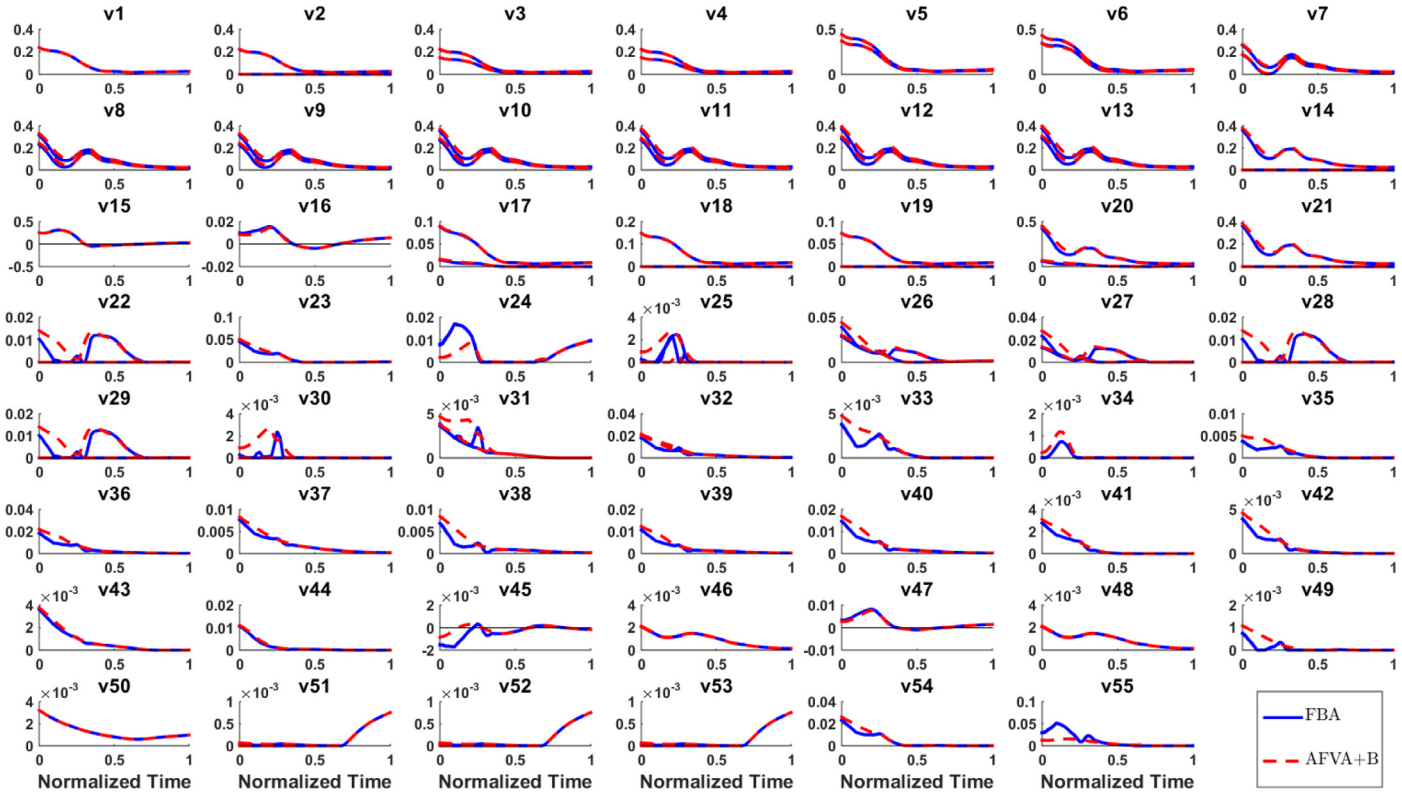

Fig. 6. Inferred fluxes (in $mmol.l^{-1}$) with FBA (blue curves) and AFVA+B (red dashed curves). (For interpretation of the references to colour in this figure legend, the reader is referred to the web version of this article.)

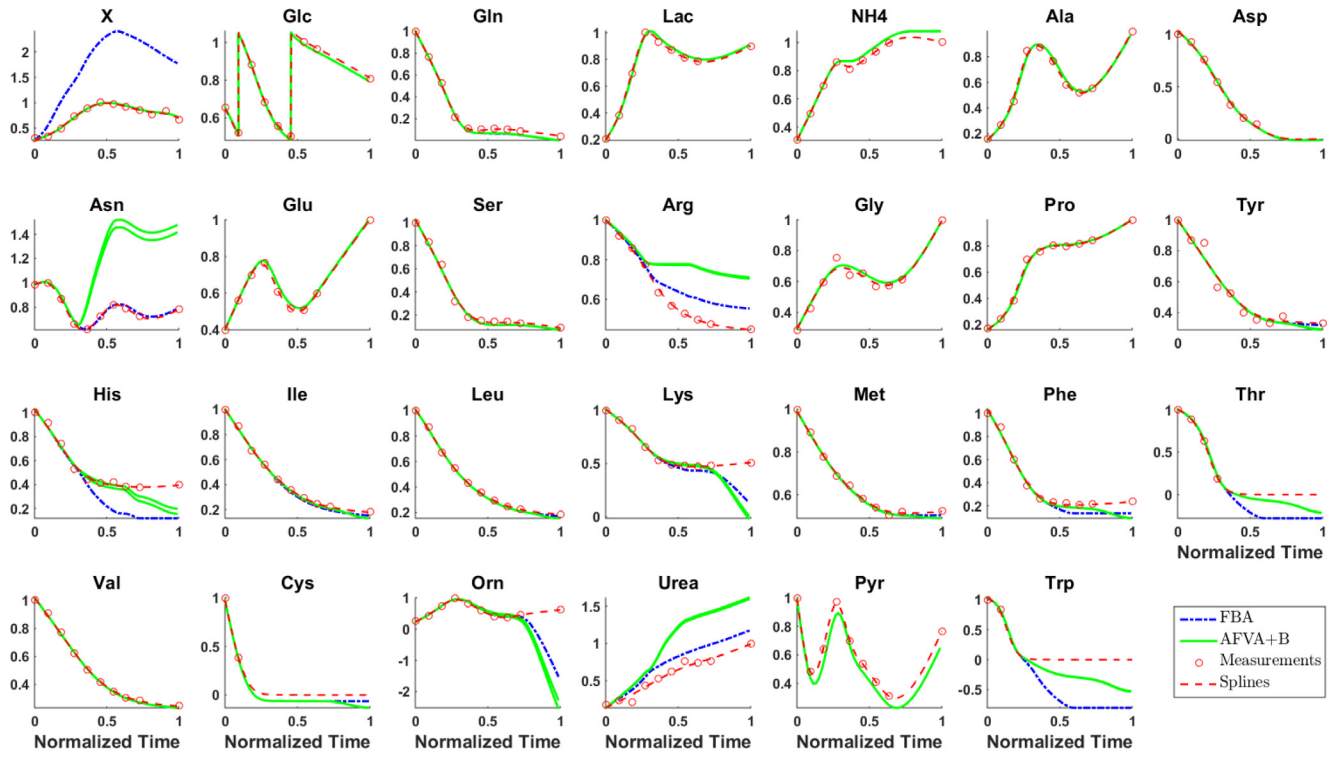

(a)

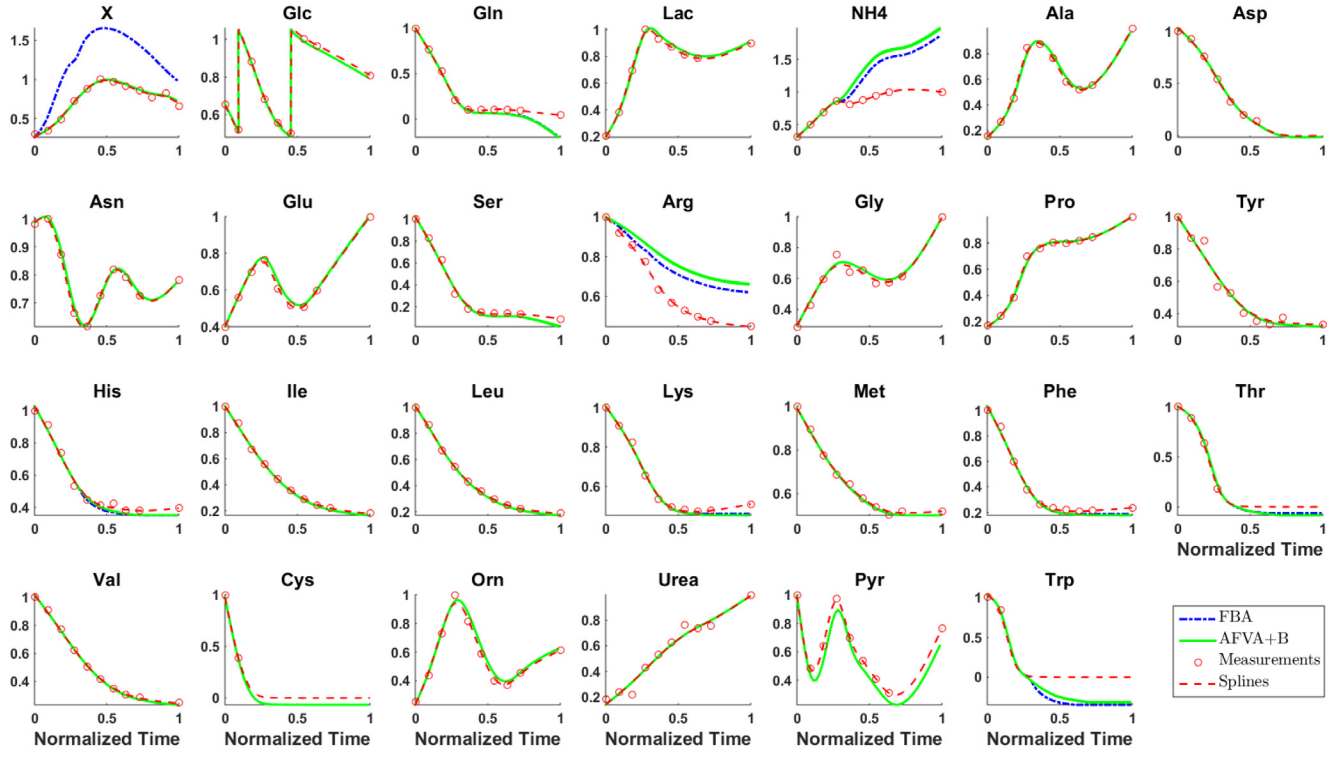

(b)

Fig. 7. Normalized external metabolite concentrations obtained through integration of the estimated flux intervals of A1 (blue curves) and A3 (green curves) compared to original smoothing splines (red dashed curves): (a) absolute coefficients of variation; (b) normalized coefficients of variation. In the latter case, the integrated curves remain in agreement with the results obtained with no biomass flux imposed. (For interpretation of the references to colour in this figure legend, the reader is referred to the web version of this article.)

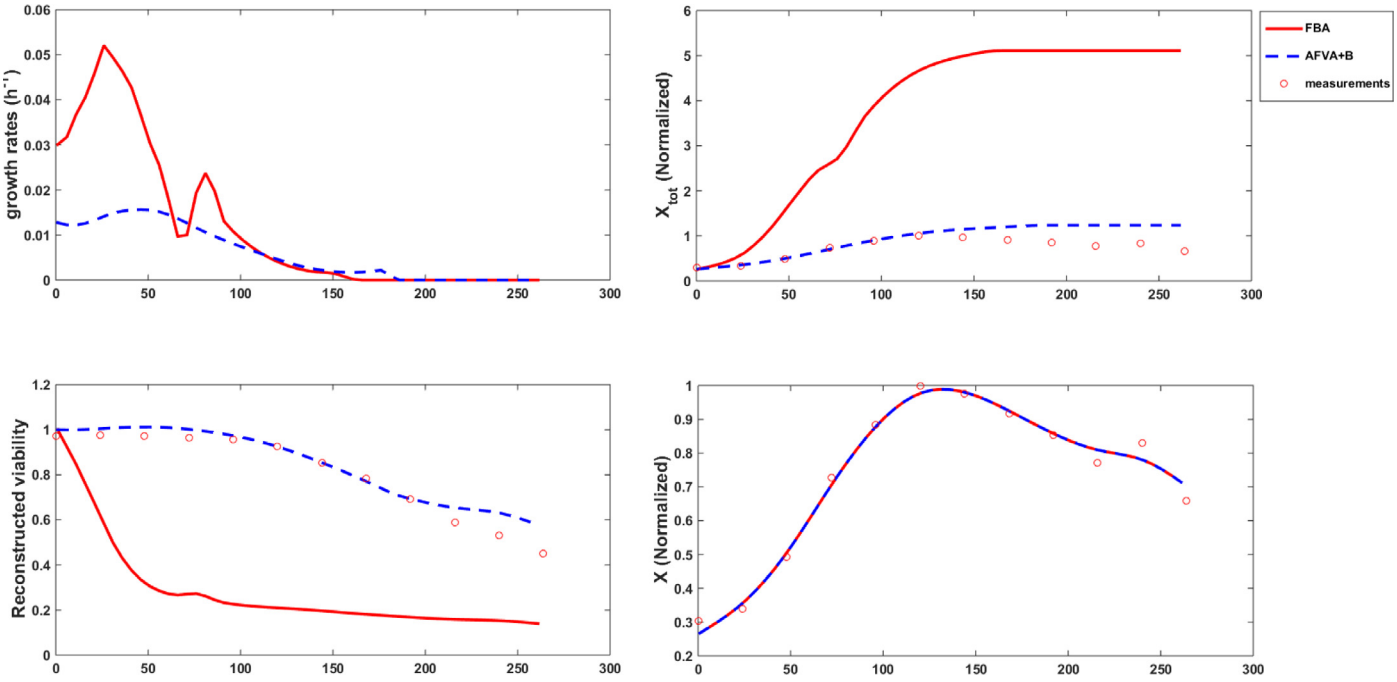

Fig. 8. Growth rates, total normalized biomass concentrations obtained by integration of the growth rate, and reconstructed viability corresponding to FBA approach and AFVA+B.

biomass (X_{tot}) along the culture, i.e. both living and dead cell populations. The dead cell concentration is therefore simply the distance between X_{tot} and the measured living cells and the viability is easily obtained using Eq. (14). In the case of FBA, the total biomass X_{tot} is far larger than the measured concentrations, and the viability signal also deviates from the measurements. It corresponds to an important drop of the viability in the early hours of the culture, which does not make sense. Conversely, the total biomass and the inferred viability signals obtained with AFVA+B are much more coherent. This stresses the gain in precision that can be expected when using AFVA+B instead of a classical FBA approach.

It should be noted that these results have been obtained with a biomass production reaction that refers to CHO cells and that the results might be further improved using a tailored reaction for biomass production.

5. Conclusions

In this work, AFVA was successfully applied to a medium size network containing 82 reactions, 51 internal metabolites as well as 27 measured external species out of 28. AFVA allowed computing the flux distribution corresponding to a rich dataset containing all 20 amino acids, as well as metabolites such as pyruvate and urea. In addition, AFVA made it possible to impose a biomass growth rate inferred from the measurements of living cells and viability as an external flux. To the best of our knowledge, this was never achieved before, except in static studies (Follstad et al., 1999) or using a FBA approach, likely because this constraint was too stringent to obtain admissible fluxes. In the present study, the results of this analysis are satisfactory and it has been shown that the biomass fluxes evaluated using AFVA are more consistent than those computed with FBA. These comforting results are obtained even though the biomass reaction actually corresponds to CHO cells instead of HEK cells, which supports the claim (Pe'er et al., 2004) that the composition of eukaryote cells is on average very similar.

In addition, this study investigates the best formulation of the error model, corresponding either to relative, absolute or normalized coefficients of variation. Although the use of absolute coefficients of variation leads to results in good agreement with the available data when the biomass flux is not imposed, a lack of robustness is observed when this latter flux is fixed. Normalized coefficients of variation usually provide robust results and are recommended.

It has also been demonstrated that data-smoothing has little impact on the quality of the evaluated flux intervals, and it is suggested to use a relatively strong data smoothing to enhance solution interpretation.

Declaration of Competing Interest

The authors declare that they have no known competing interest that could have influenced the work reported in this article.

Acknowledgment

The authors are very grateful to GlaxoSmithKline who provided the datasets used in this study, as well as material and financial support to the first author, in the accomplishment of his PhD thesis at the University of Mons, under a joint research project.

Supplementary material

Supplementary material associated with this article can be found, in the online version, at doi:10.1016/j.compchemeng.2019.106633.

References

Abbate, T., Dewasme, L., Bogaerts, P., Wouwer, A.V., 2019. Adaptive flux variability analysis: a tool to deal with uncertainties. IFAC-PapersOnLine 52 (1), 70–75.
Bastin, G., 2016. Quantitative analysis of metabolic networks and design of minimal bioreaction models. Rev. Afr. Rech. Inf. Math. Appl. 9.
Bogaerts, P., Gziri, K.M., Richelle, A., 2017. From MFA to FBA: defining linear constraints accounting for overflow metabolism in a macroscopic FBA-based dynamical model of cell cultures in bioreactor. J. Process Control 60, 34–47.

Duarte, N.C., Becker, S.A., Jamshidi, N., Thiele, I., Mo, M.L., Vo, T.D., Srivas, R., Palsson, B.Ø., 2007. Global reconstruction of the human metabolic network based on genomic and bibliomic data. Proc. Natl. Acad. Sci. 104 (6), 1777–1782. doi:10.1073/pnas.0610772104.

Fernandes, S., Robitaille, J., Bastin, G., Jolicoeur, M., Vande Wouwer, A., 2016. Application of dynamic metabolic flux convex analysis to CHO-DXB11 cell fed-batch cultures. IFAC-PapersOnLine 49 (7), 466–471.

Follstad, B.D., Balcarcel, R.R., Stephanopoulos, G., Wang, D.I., 1999. Metabolic flux analysis of hybridoma continuous culture steady state multiplicity. Biotechnol. Bioeng. 63 (6), 675–683.

Heath, C., Kiss, R., 2007. Cell culture process development: advances in process engineering. Biotechnol. Prog. 23 (1), 46–51.

Henry, O., Jolicoeur, M., Kamen, A., 2011. Unraveling the metabolism of HEK-293 cells using lactate isotopomer analysis. Bioprocess Biosyst. Eng. 34 (3), 263–273.

Henry, O., Perrier, M., Kamen, A., 2005. Metabolic flux analysis of HEK-293 cells in perfusion cultures for the production of adenoviral vectors. Metab. Eng. 7 (5–6), 467–476.

Kanehisa, M., Furumichi, M., Tanabe, M., Sato, Y., Morishima, K., 2016. Kegg: new perspectives on genomes, pathways, diseases and drugs. Nucleic Acids Res. 45 (D1), D353–D361.

Karengera, E., Durocher, Y., De Crescenzo, G., Henry, O., 2017. Combining metabolic and process engineering strategies to improve recombinant glycoprotein production and quality. Appl. Microbiol. Biotechnol. 101 (21), 7837–7851. doi:10.1007/s00253-017-8513-0.

Kauffman, K.J., Prakash, P., Edwards, J.S., 2003. Advances in flux balance analysis. Curr. Opin. Biotechnol. 14 (5), 491–496.

Klamt, S., Stelling, J., 2003. Two approaches for metabolic pathway analysis? Trends Biotechnol. 21 (2), 64–69.

Leighty, R.W., Antoniewicz, M.R., 2011. Dynamic metabolic flux analysis (DMFA): a framework for determining fluxes at metabolic non-steady state. Metab. Eng. 13 (6), 745–755.

Llaneras, F., Picó, J., 2007. An interval approach for dealing with flux distributions and elementary modes activity patterns. J. Theor. Biol. 246 (2), 290–308.

Llaneras, F., Picó, J., 2008. Stoichiometric modelling of cell metabolism. J. Biosci. Bioeng. 105 (1), 1–11.

Llaneras, F., Sala, A., Picó, J., 2012. Dynamic estimations of metabolic fluxes with constraint-based models and possibility theory. J Process Control 22 (10), 1946–1955.

Mahadevan, R., Edwards, J.S., Doyle III, F.J., 2002. Dynamic flux balance analysis of diauxic growth in Escherichia coli. Biophys. J. 83 (3), 1331–1340.

Mahadevan, R., Schilling, C., 2003. The effects of alternate optimal solutions in constraint-based genome-scale metabolic models. Metab. Eng. 5 (4), 264–276.

Martinez, V., Gerdtzen, Z., Andrews, B.A., Asenjo, J.A., 2010. Viral vectors for the treatment of alcoholism: use of metabolic flux analysis for cell cultivation and vector production. Metab. Eng. 12 (2), 129–137.

Papin, J.A., Stelling, J., Price, N.D., Klamt, S., Schuster, S., Palsson, B.O., 2004. Comparison of network-based pathway analysis methods. Trends Biotechnol. 22 (8), 400–405.

Pe'er, I., Felder, C.E., Man, O., Silman, I., Sussman, J.L., Beckmann, J.S., 2004. Proteomic signatures: amino acid and oligopeptide compositions differentiate among phyla. Proteins Struct. Funct. Bioinf. 54 (1), 20–40.

Petiot, E., Cuperlovic-Culf, M., Shen, C.F., Kamen, A., 2015. Influence of hek293 metabolism on the production of viral vectors and vaccine. Vaccine 33 (44), 5974–5981. doi:10.1016/j.vaccine.2015.05.097. Vaccine Engineering

Price, N.D., Reed, J.L., Palsson, B.Ø., 2004. Genome-scale models of microbial cells: evaluating the consequences of constraints. Nat. Rev. Microbiol. 2 (11), 886.

Provost, A., Bastin, G., 2004. Dynamic metabolic modelling under the balanced growth condition. J Process Control 14 (7), 717–728.

Quek, L.-E., Dietmair, S., Hanscho, M., Martínez, V.S., Borth, N., Nielsen, L.K., 2014. Reducing recon 2 for steady-state flux analysis of HEK cell culture. J. Biotechnol. 184, 172–178.

Ravi, M., Paramesh, V., Kaviya, S., Anuradha, E., Solomon, F.P., 2015. 3d cell culture systems: advantages and applications. J. Cell. Physiol. 230 (1), 16–26.

Richelle, A., Gziri, K.M., Bogaerts, P., 2016. A methodology for building a macroscopic FBA-based dynamical simulator of cell cultures through flux variability analysis. Biochem. Eng. J. 114, 50–64.

Stephanopoulos, G., Aristidou, A.A., Nielsen, J., 1998. Metabolic Engineering: Principles and Methodologies. Academic Press.

Thiele, I., Palsson, B.Ø., 2010. A protocol for generating a high-quality genome-scale metabolic reconstruction. Nat. Protoc. 5 (1), 93.

Trinh, C.T., Wlaschin, A., Srienc, F., 2009. Elementary mode analysis: a useful metabolic pathway analysis tool for characterizing cellular metabolism. Appl. Microbiol. Biotechnol. 81 (5), 813.

Vercammen, D., Logist, F., Van Impe, J., 2014. Dynamic estimation of specific fluxes in metabolic networks using non-linear dynamic optimization. BMC Syst. Biol. 8 (1), 132.

Zamorano, F., Vande Wouwer, A., Jungers, R.M., Bastin, G., 2013. Dynamic metabolic models of CHO cell cultures through minimal sets of elementary flux modes. J. Biotechnol. 164 (3), 409–422.